The challenging physics regimes of high current electron beams

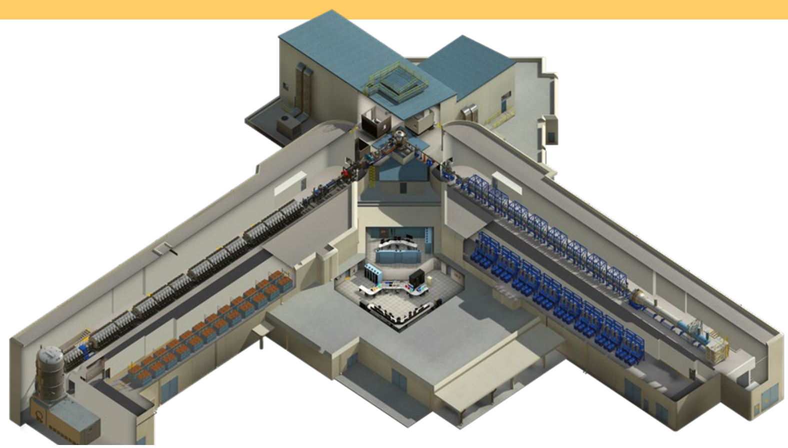

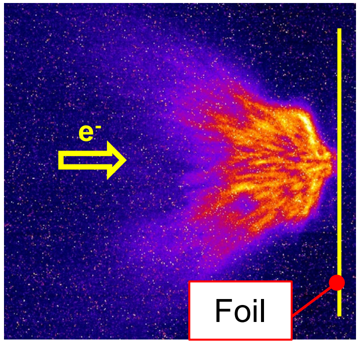

J.E. Coleman, C.A. Ekdahl, J.E. Koglin, <u>S.M. Lund</u>, D.C. Moir, H.E. Morris, N.B. Ramey, and <u>P.A. Seidl</u>

Los Alamos National Laboratory, Los Alamos, NM, United States

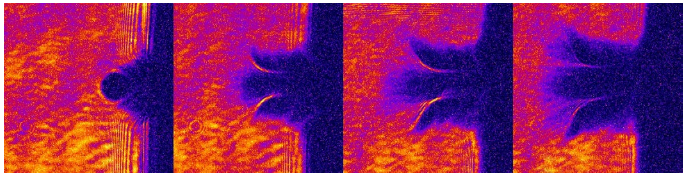

Dual-axis radiographic hydrodynamic test (DARHT) is the world’s premier radiographic facility.

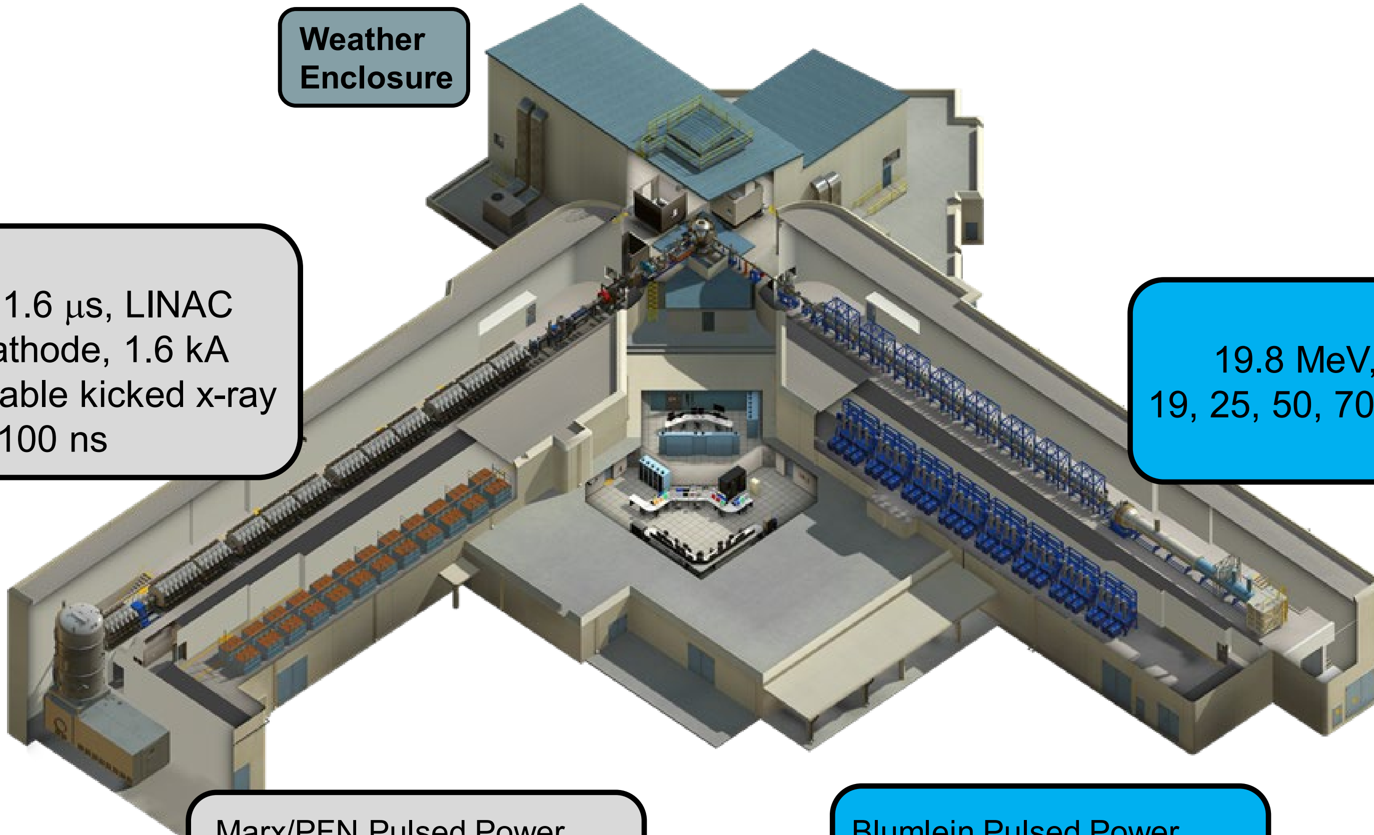

Axis-II
16.5 MeV, 1.6 μs, LINAC
165 mm cathode, 1.6 kA
Programmable kicked x-ray pulses 20-100 ns

Axis-I
19.8 MeV, 80 ns FWHM
19, 25, 50, 70 mm cathodes
0.26 - 2.9 kA

Marx/PFN Pulsed Power
Thermionic cathode
Metglas Induction Cell cores

Blumlein Pulsed Power
Velvet cathode
Ferrite Induction Cell Cores

Two fundamentally different electron induction accelerators are used to obtain orthogonal radiographs of fully contained hydrodynamic tests at multiple times.

There are 3 separate regions in our induction accelerators where challenging physics is available to study.

DARHT Axis-1

Accelerator 8 Cell Blocks; 64, 250 kV Cells

Injector

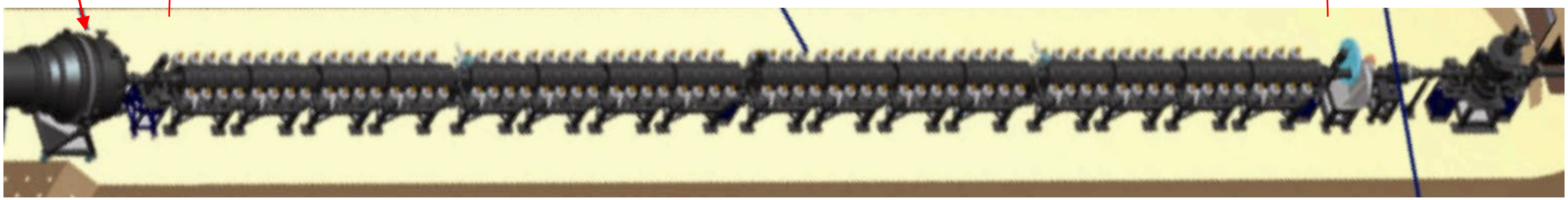

Injector transport

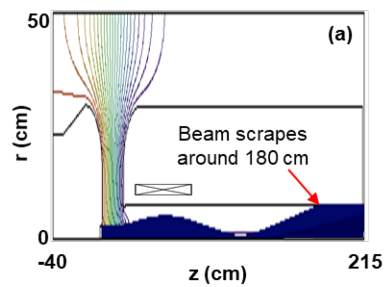

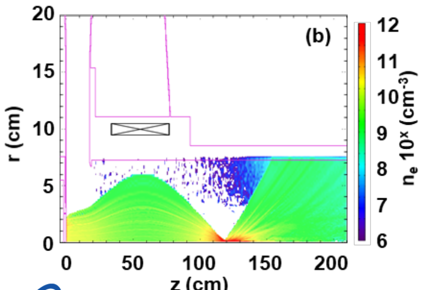

Accelerator transport physics

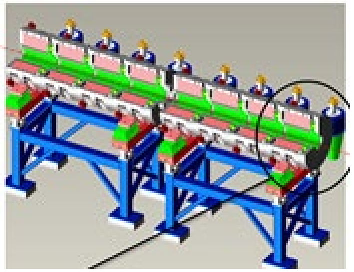

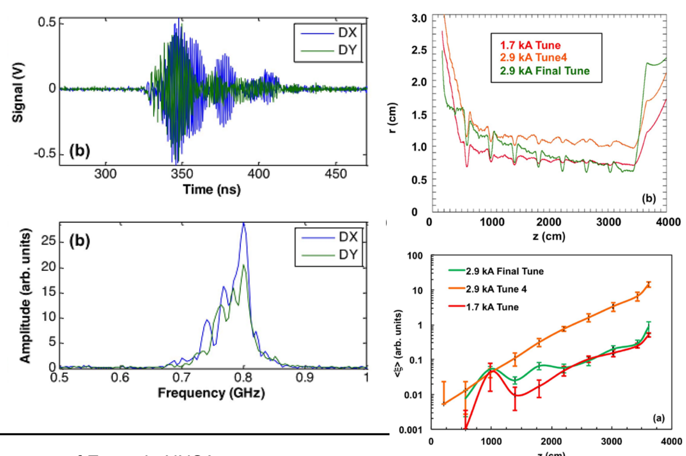

Target interaction physics

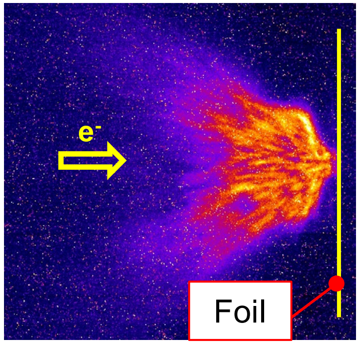

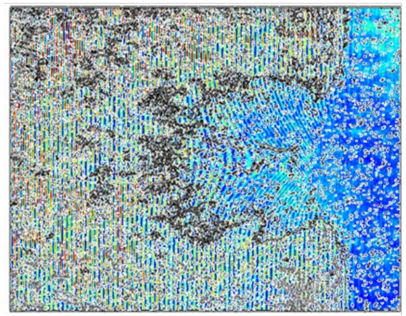

Cathode & injector transport physics

Cathode technology example: Electrons produced via field emission from velvet fibers.

Early velvet cathodes tests by Adler[1], 30 kV, 690 A and Gilgenbach[2] 600 kV, 8 kA

Flashover threshold 16 kV/cm [3]

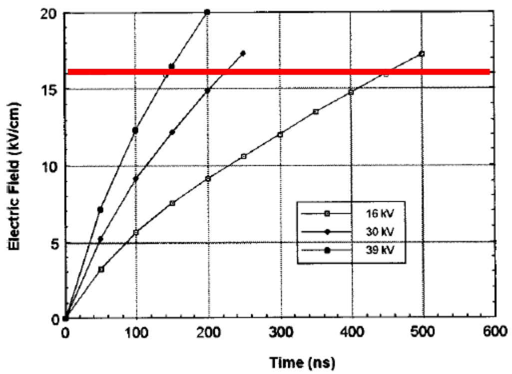

Threshold for the appearance of electron emission to be E = 8 ± 1 kV/cm. [4]

7 kV, 3 A, d_{fiber} = 8 um, d_{AK} = 3 cm [4]

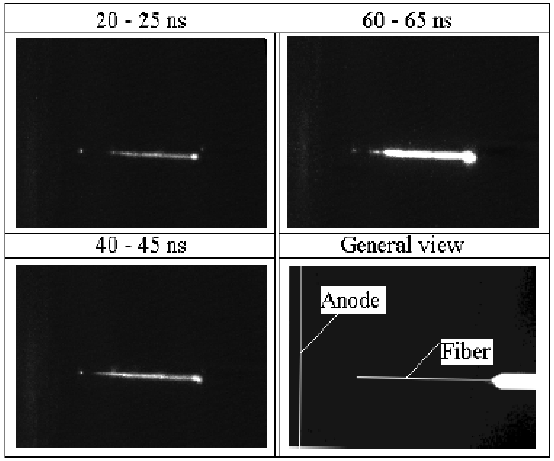

5 cm velvet cathode

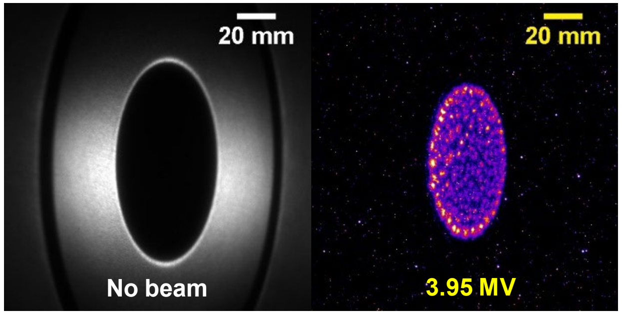

Field emission & H_α emission

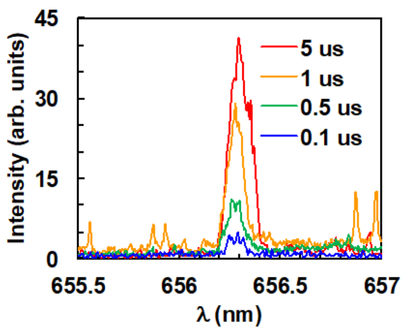

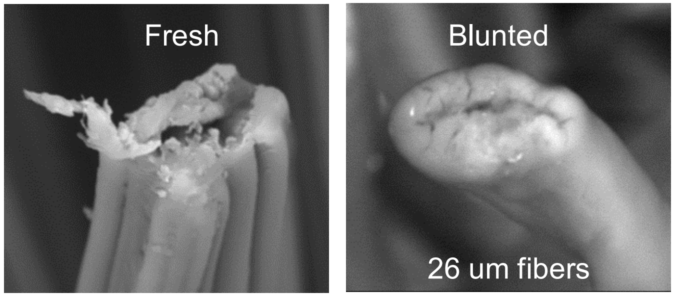

[1] R.J. Adler et al., Rev. Sci. Instrum. **56**, 766 (1985).
[2] R.M. Gilgenbach et al., Proceedings of the 5th International Pulsed Power Conference, Crystal City, VA, 1985.
[3] R.B. Miller, J. Appl. Phys. **84**, 3880 (1998).
[4] Y.E. Krasik, A. Dunaevsky, and J. Felsteiner, Eur. Phys. J. D **15**, 345 (2001).
[5] J.E. Coleman et al., Phys. Plasmas **22**, 033508 (2015).

Detailed diode modeling has been conducted on the effects of the velvet cathode recess on emission.

EPURE Axis-1 diode, $d_{cathode}$ = 3.2 cm, d_{AK} = 17.2 cm

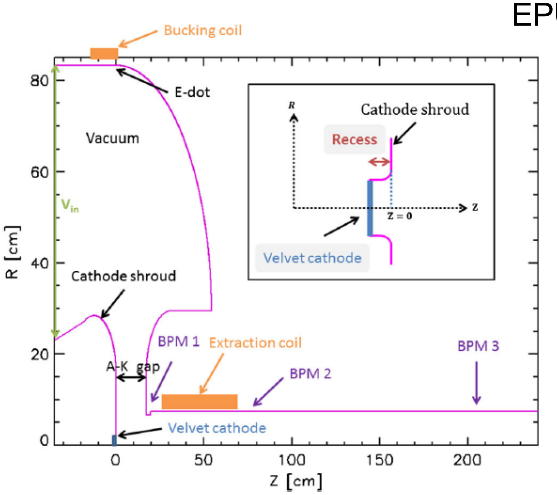

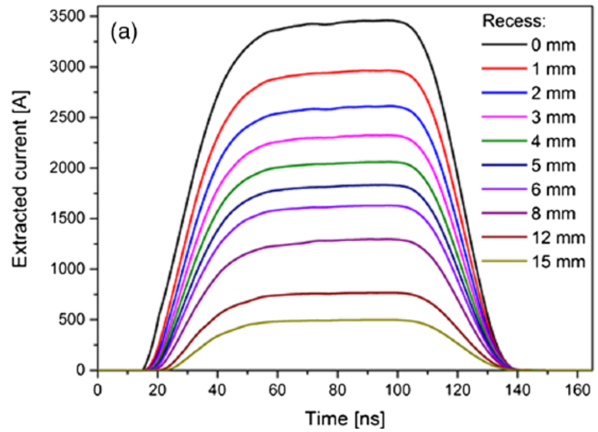

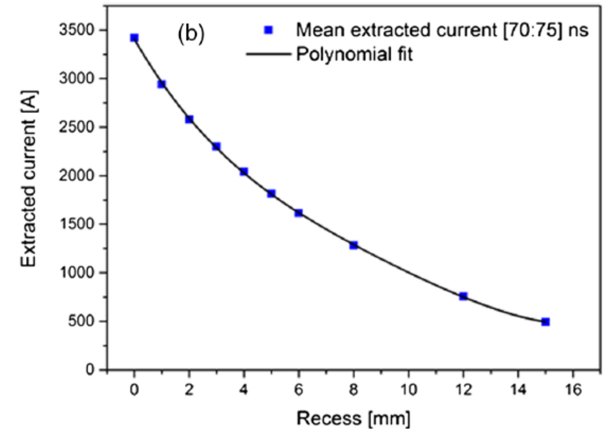

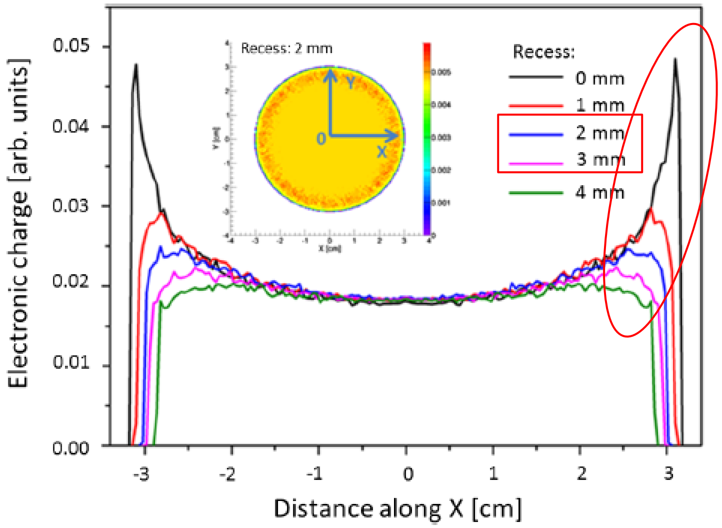

Hollow beam current densities are pronounced on smaller cathodes

This can lead to diocotron

J.M. Plewa et al., Phys. Rev. Accel. Beams **21**, 070401 (2018).

Cathode illumination, ionized monolayers of hydrogen (H_α), indicate enhanced edge emission with smaller cathodes.

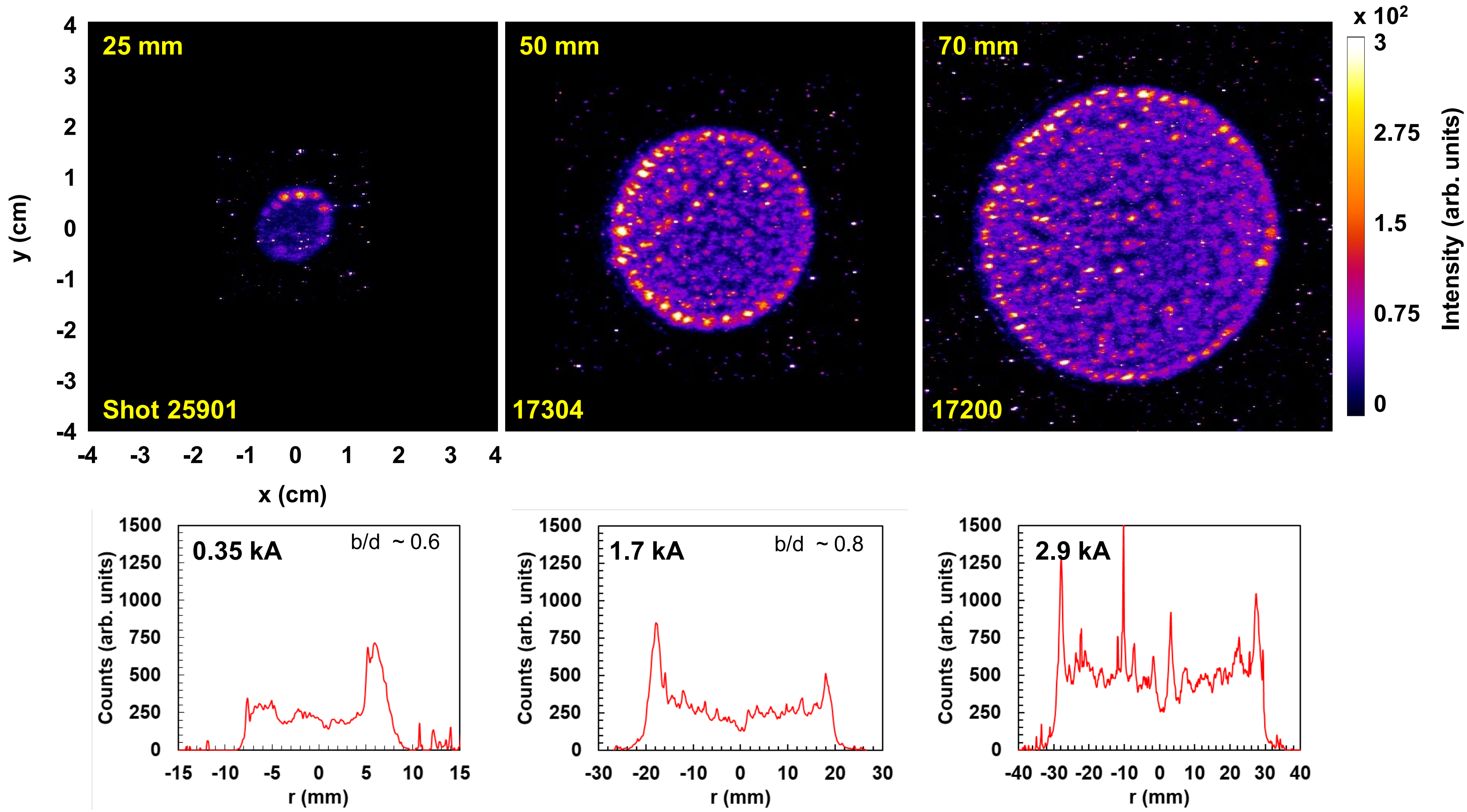

Unintentionally create a hollow, => unstable beam transport

Hollow electron beams transported in a magnetic field are susceptible to a velocity shear – Diocotron instability

Webster made the first experimental observation of the diocotron instability (*Breakup of hollow e- beams*) [1]

15.6 V, 200 mA, 340 G

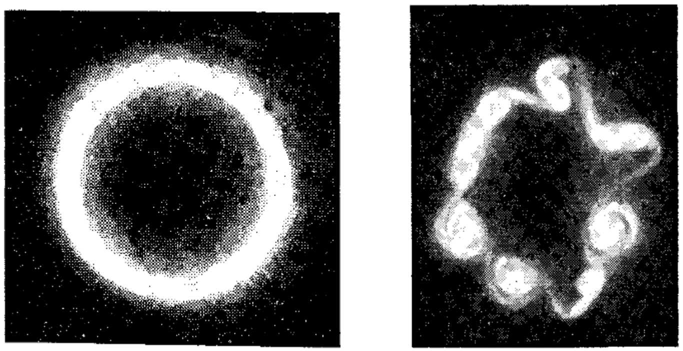

J(x,y) at 1 cm   8.7 cm

Diocotron (cylindrical) is synonymous with Kelvin-Helmholtz

Hollow electron beam => different angular velocities due to focusing of the solenoid

- focusing force is stronger for lower current density beam -> **higher v_ϕ**

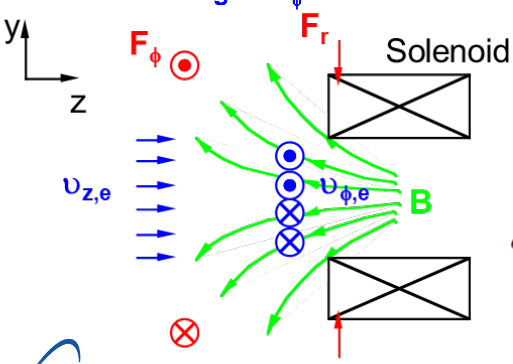

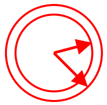

b – inner circle diameter
d – outer circle diameter

Diocotron Frequency $\Omega_D = \dfrac{\omega_{pe}^2}{2\omega_{ce}}$

$$F_r = F_{cent} + F_{SC}$$

$$qwrB_z = m\omega^2 r + \frac{Kmv_z^2 r}{a^2}.$$

$$\omega_p = \sqrt{\frac{nq^2}{\epsilon_o m}}, \quad \omega_c = \frac{qB}{m}.$$

Growth rate [2]

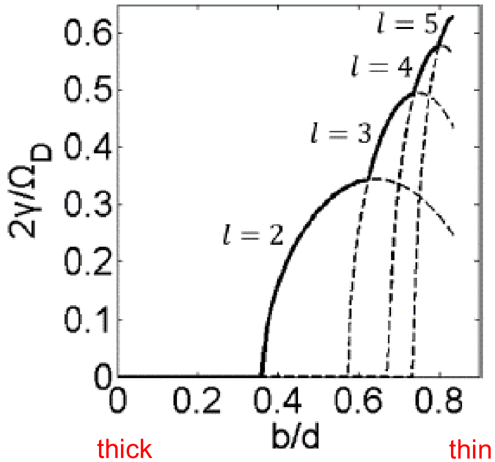

[1] H.F. Webster, J. Appl. Phys. **26**, 1386 (1955).
[2] Y.H. Jo et al., Phys. Plasmas **25**, 011607 (2018).

Small cathodes indicate evidence of the onset of an instability when mildly focused – Diocotron?

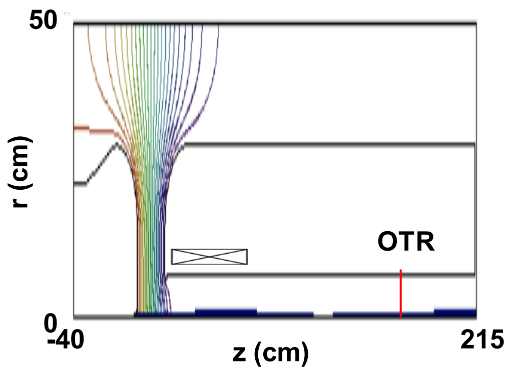

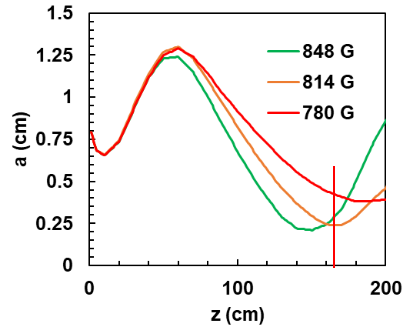

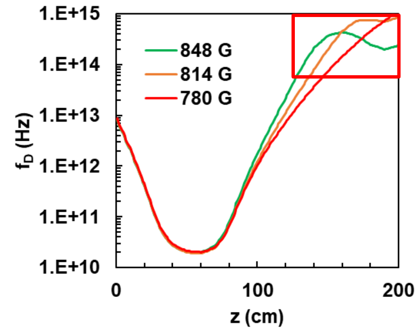

$$f_D = \frac{f_{pe}^2}{2 f_{ce}}$$

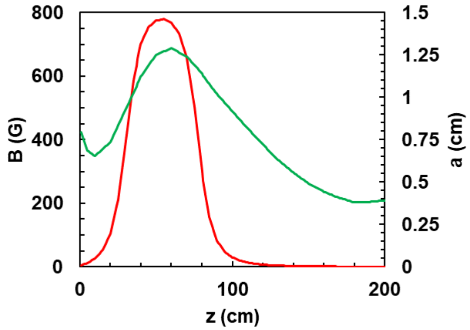

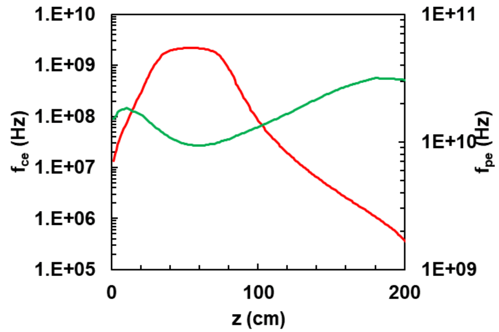

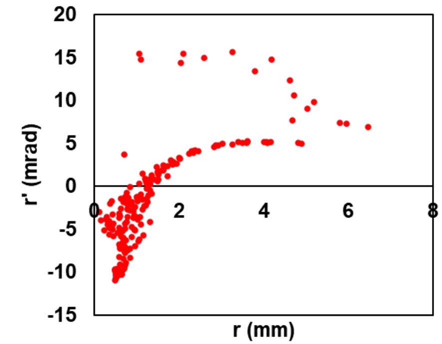

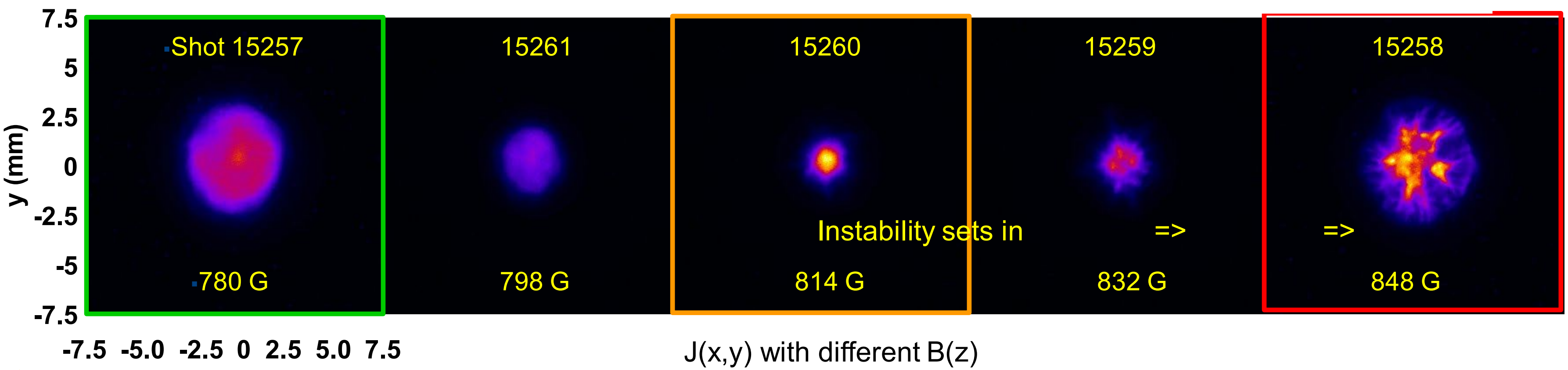

J(x,y) with different B(z)

Beam transport physics

Misalignments of induction accelerator transport elements can contribute to poor beam quality.

Axis-1: we measure non-uniform distributions directly out of the gun & a substantial halo through the accelerator

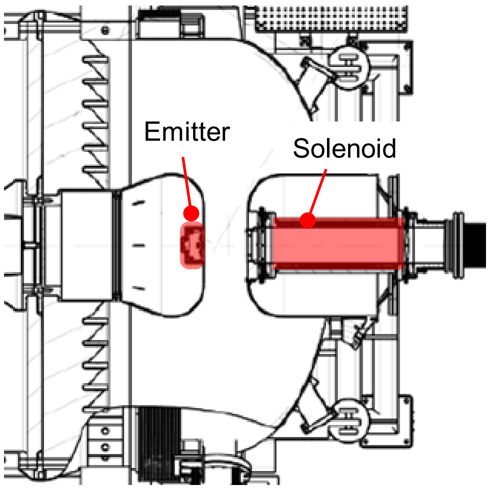

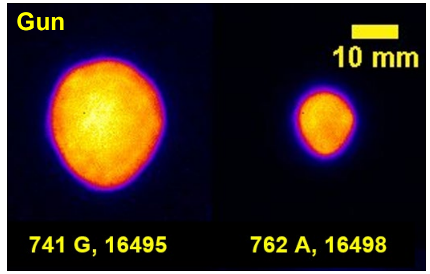

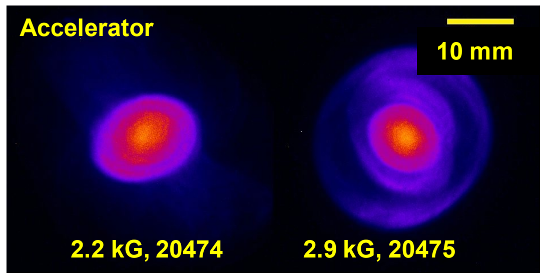

ε_n (mm-mrad) growth details

Axis-1	Gun	Accelerator
1.9 cm	400	680
5 cm	800	2000
7 cm	1500	not meaured
Axis-2		
16.5 cm	254	811

>2x $\Delta\varepsilon$

>3x $\Delta\varepsilon$

Induction cell

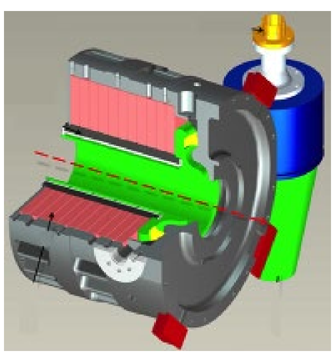

Individual misalignments

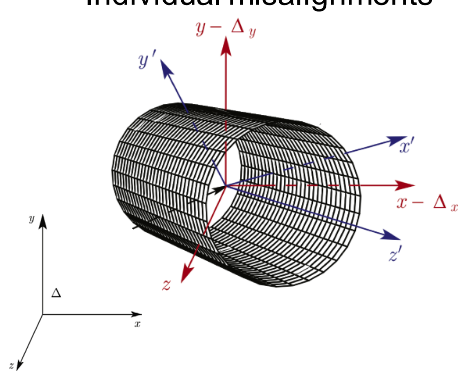

Mismatched beam envelope [3]

$$\eta = (r - r_m)/r_m,$$

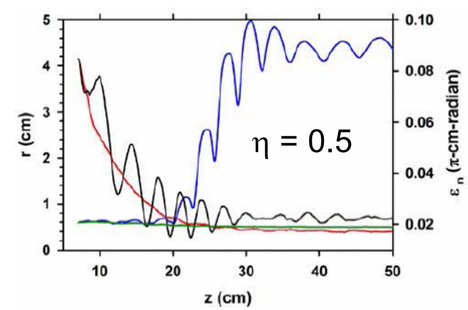

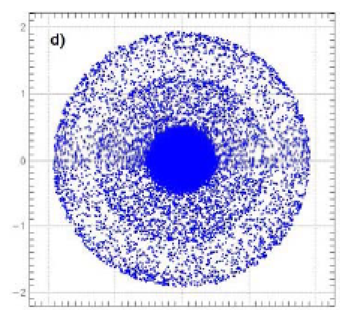

[1] Y.-J. Chen et al., in Proceedings of the Particle Accelerator Conference, San Francisco, CA, 1991, p. 3100.
[2] J.E. Coleman et al., Phys. Rev. ST Accel. Beams **17**, 092802 (2014).
[3] C.A. Ekdahl et al., IEEE Trans. Plasma Sci. **45**, 2962 (2017).

Betatron oscillations of the beam centroid are captured along the accelerator lattice.

Solenoid lattice, Tune 4, 3/19/2013

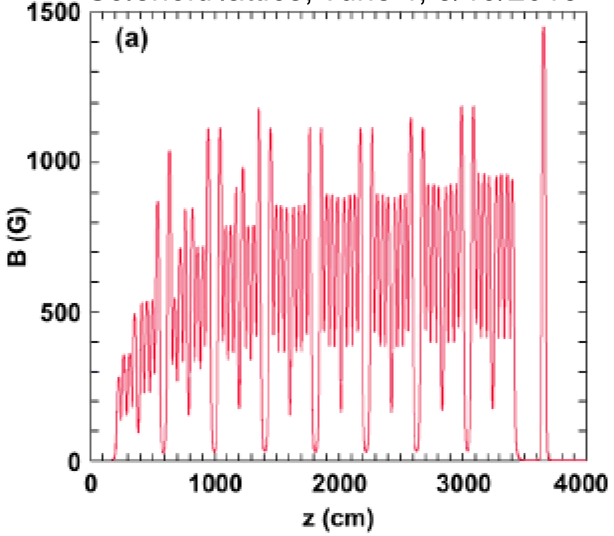

Betatron wavelength, λ_β

$$\lambda_\lambda = \beta c\ (2\pi/\omega_\lambda).$$

$$\lambda_b = L\ (2\pi/\mu_o). \qquad \mu_o = \cos^{-1}(TrM/2).$$

$$\lambda_\beta = \frac{4\pi m_e \beta\gamma c}{qB_z} = \frac{4\pi\beta\gamma c}{\omega_{ce}} = \frac{2\pi}{k_\beta}$$

Betatron wavenumber, k_β

$$k_\beta = \frac{2\pi B_z}{\mu_0 I_A} \qquad k_\beta = \frac{qB_z}{2m_e\beta\gamma c}$$

Shot 16445 – Tune4

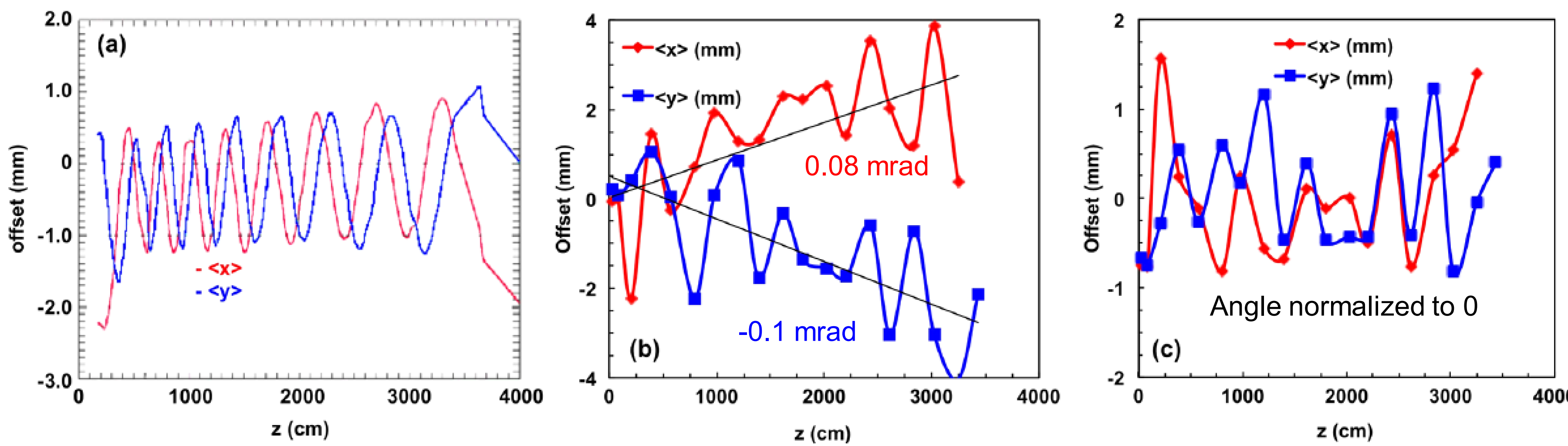

J.E. Coleman et al., Phys. Rev. ST Accel. Beams **17**, 092802 (2014).
Stanley Humphries Jr., Charged Particle Beams, John Wiley and Sons Inc., New York, Ch. 1 p. 17 (2002).

Solenoid lattice iterations can significantly impact the beam dynamics; enough information can be gathered to determine lattice element misalignments.

Effective Larmor rotation

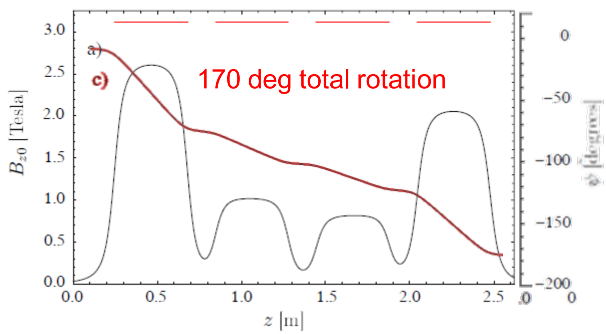

Statistical contributions of individual misalignments

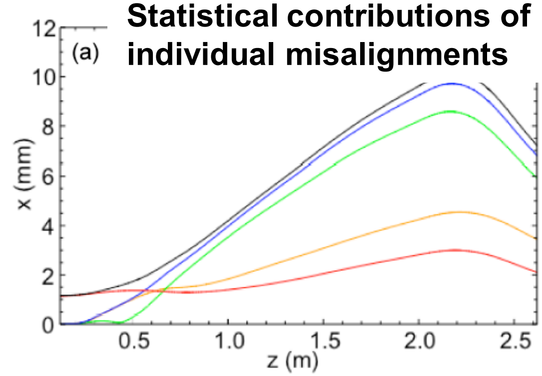

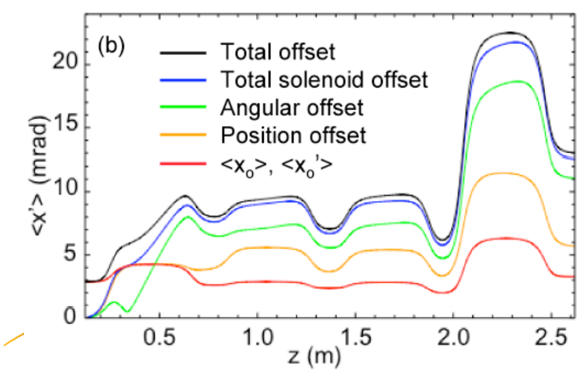

Example Lattice Iterations

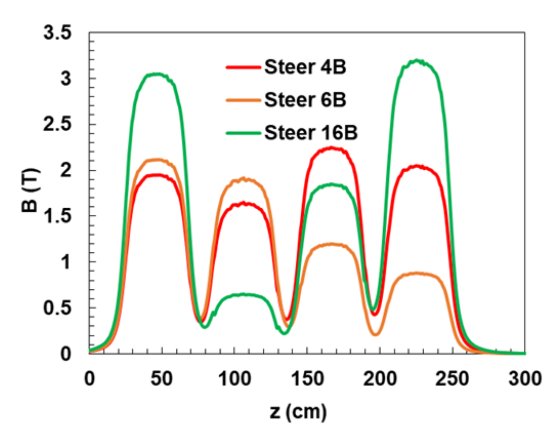

Measured Centroid

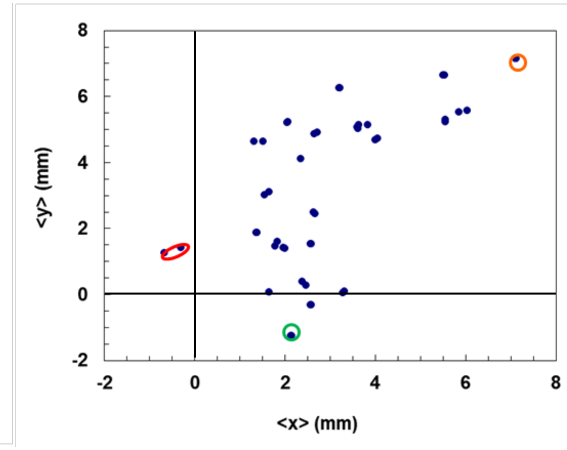

Steer 4B **Steer 16B** **Steer 6B**

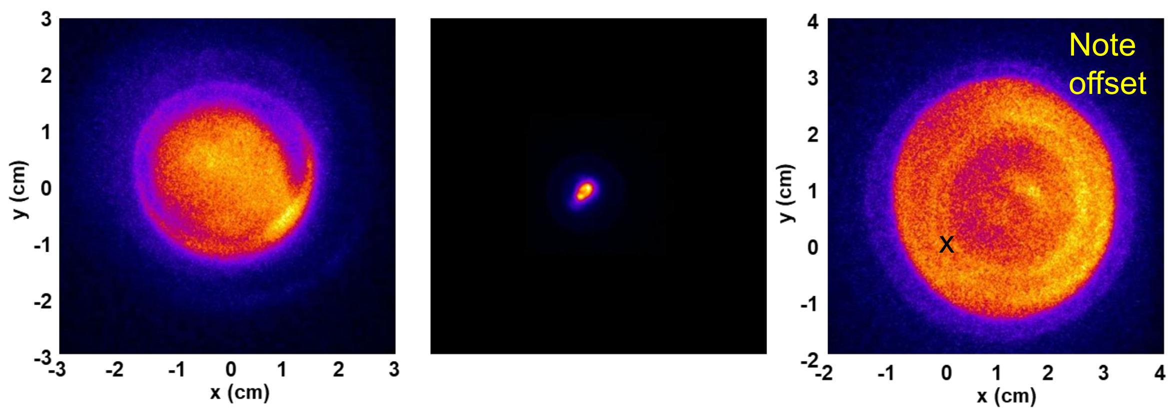

A facility could be setup to educate/develop students - beam transport

[1] S.M. Lund et al., Nucl. Instrum. Methods Phys. Res., Sect. A 606, 56 (2009).
[2] S. M. Lund et al., in Proceedings 23rd Particle Accelerator Conference, 2009 p. 4323.
[3] J. E. Coleman, Ph.D. Thesis, University of California, Berkeley, 2008.

Beam break-up (BBU) was first observed on SLAC nearly 60 years ago and continues to be a transport limit.

DARHT Axis-1 Shot 17139

Observations at SLAC (1966)

Increasing current

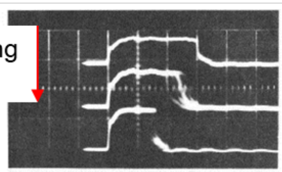

(Top) Beam current below BBU threshold and above BBU threshold (bottom)

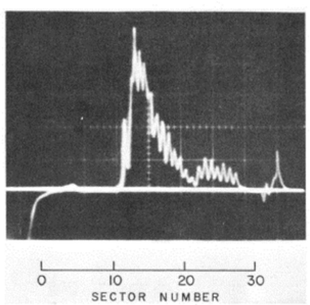

Fig. 3. PLIC profile for beam break-up at sector 12 (5 GeV, 1.6 μsec).

Ionization caused by lost electrons at collimators

Observations on ATA (1986)

B-dot loop

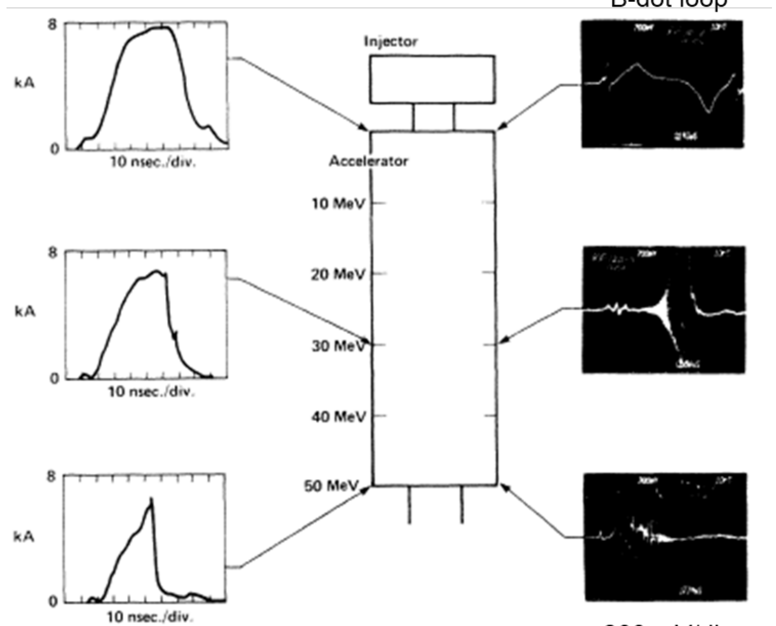

200 mV/div
10 ns/div

BPM 19

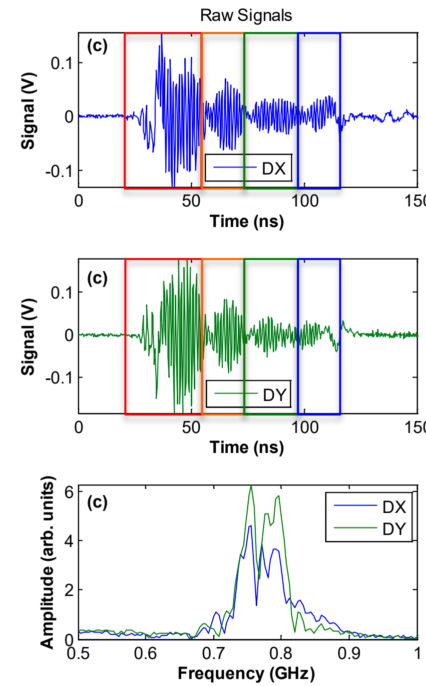

33.9 ns
18.6 ns
23.7 ns
18.6 ns

$$t = \frac{2\Gamma_m Q}{\omega}$$

Beam breakup instability (BBU)

BBU Growth $\frac{\xi(z)}{\xi_o} = \left(\frac{\gamma_o}{\gamma}\right)^{1/2} exp\Gamma_m$

BBU Growth Factor $\Gamma_m = \frac{1}{c} I_b N_g Z_\perp \left\langle \frac{1}{B} \right\rangle$

I_b – beam current
N_g – number of gaps
B – magnetic field

M.G. Kelliher and R. Beadle, Nature (London) 187, 1099 (1960).
O.H. Altenmueller *et al.,* Proc. 1966 Linear Accelerator Conf. LA-3609 (1966).
W.K.H. Panofsky and M. Bander, Rev. Sci. Instrum. 39, 206 (1968).
V. K. Neil, L. S. Hall, and R. K. Cooper, Part. Accel. 9, 213 (1979).
G. J. Caporaso et al., Phys. Rev. Lett. **57**, 1591 (1986).
J.E. Coleman et al., Phys. Rev. ST Accel. Beams **17**, 092802 (2014).

Target physics

Electron energy is deposited into our targets through a stopping power process.

DARHT Axis-1 beam parameters: 19.8 MeV, 1.4-1.7 kA

Radiographic targets are 0.2 – 1.0 mm-thick-Ta

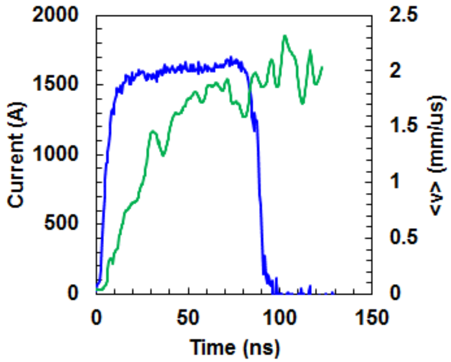

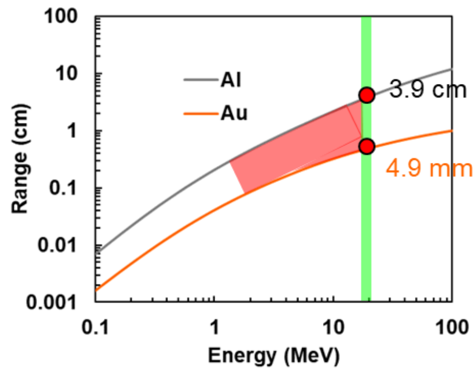

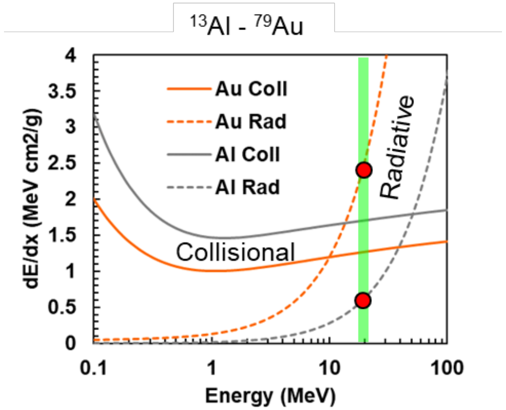

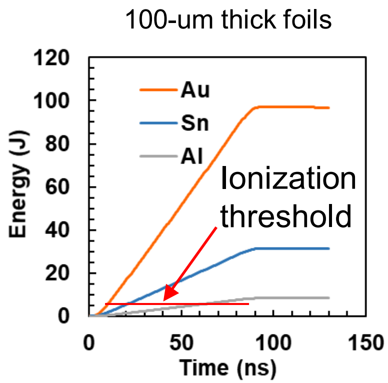

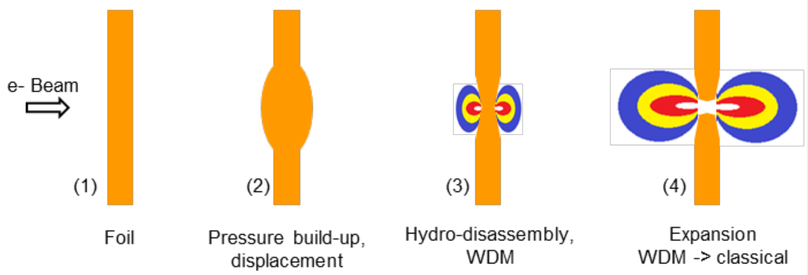

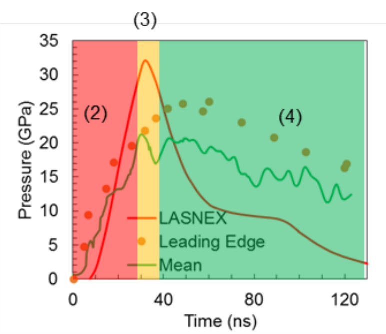

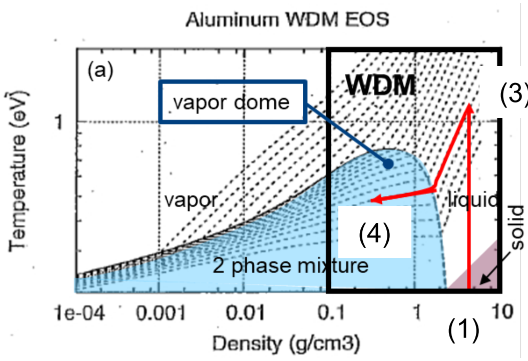

WDM – warm dense matter

Electrical conductivity (σ)
Thermal conductivity (κ)

J.E. Coleman, et al. Phys. Rev. E **98**, 043201 (2018).

The hydrodynamic disassembly timescale depends on several factors.

- **Energy density**

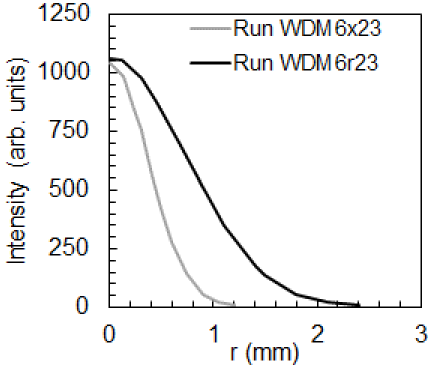

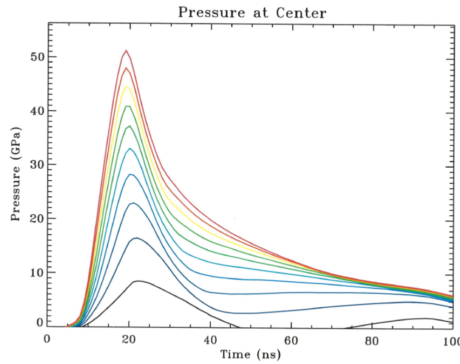

- **Material thickness**

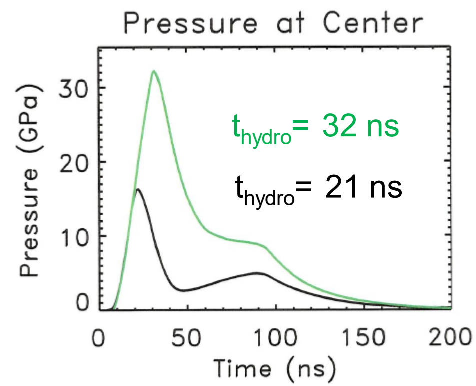

- **Material properties, phase diagrams**

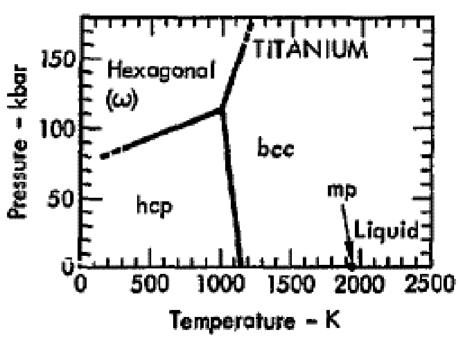

T_{melt} = 1933 K
E_{ion} = 4.9 J

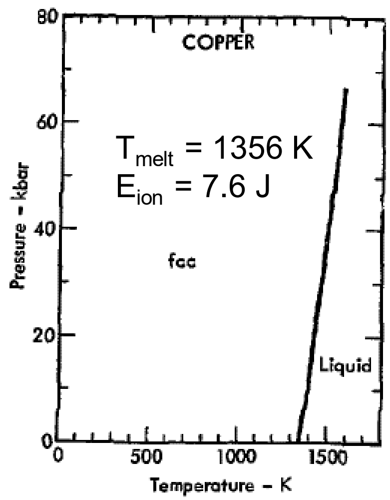

- **Target geometry**

Single Foil or other iterations

Assuming the energy is concentrated in an ideal $7.8x10^{-5}$ cm^3 cylinder.

Collisional particle beam heating is more efficient in low-Z materials at 4 MeV.

Incoming beam parameters: 1.45 kA, 1.8 mm FWHM
19.8 MeV, 2.3 kJ; 4 MeV 460 J

LASNEX, Cu EOS 3336

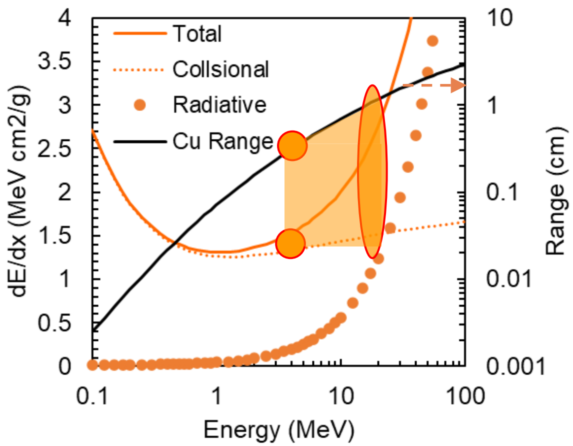

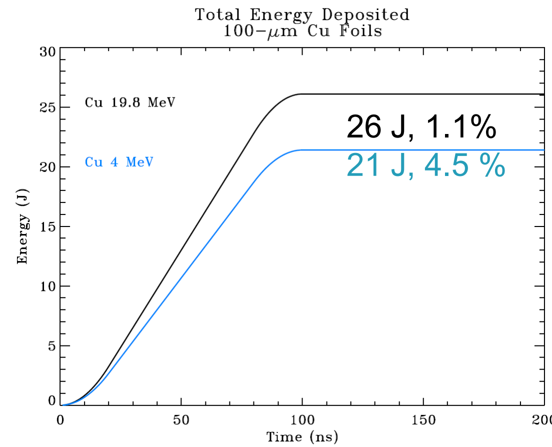

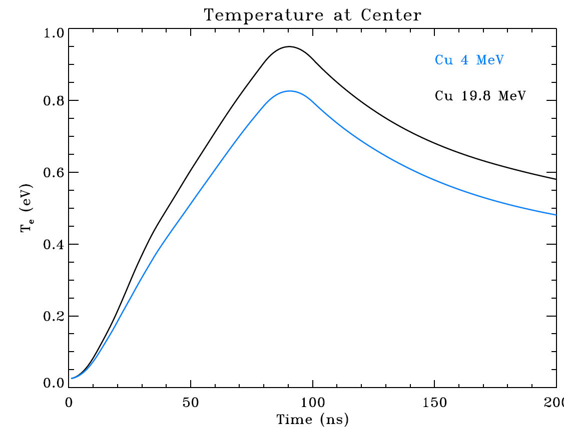

Expanded T_e & n_e at 200 ns

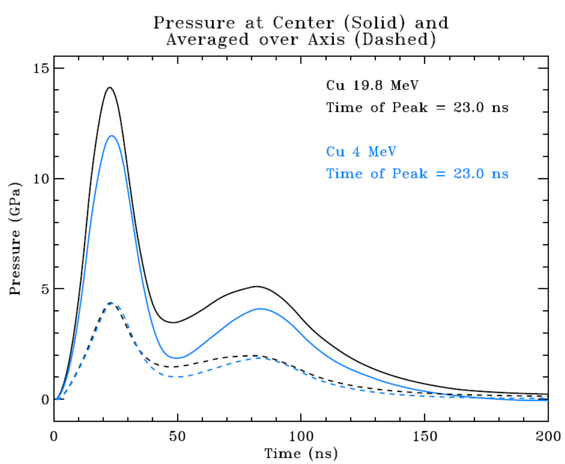

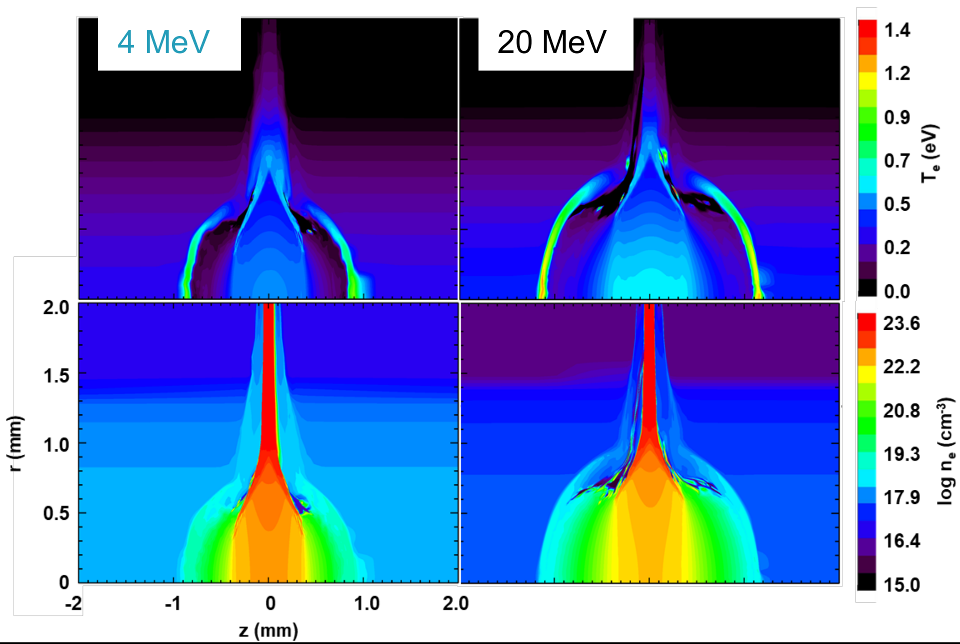

A shadowgraph and shearing interferometer was developed to measure the hydro motion & $n_e < 10^{20}$ cm^{-3} of our targets.

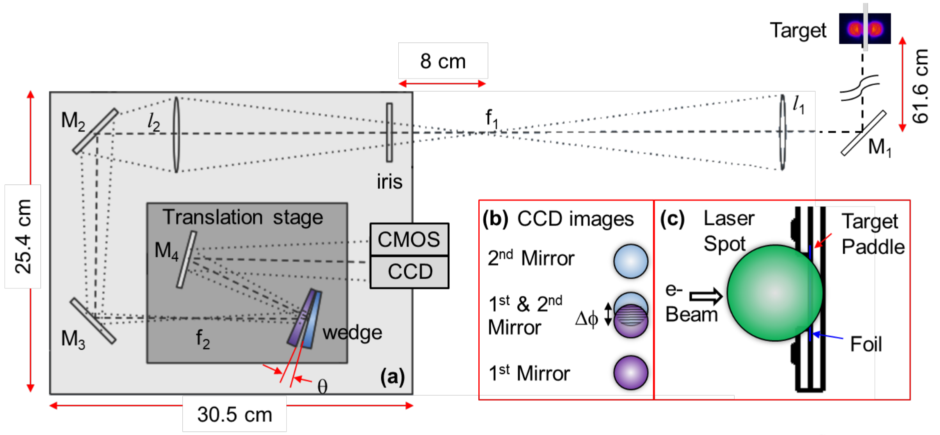

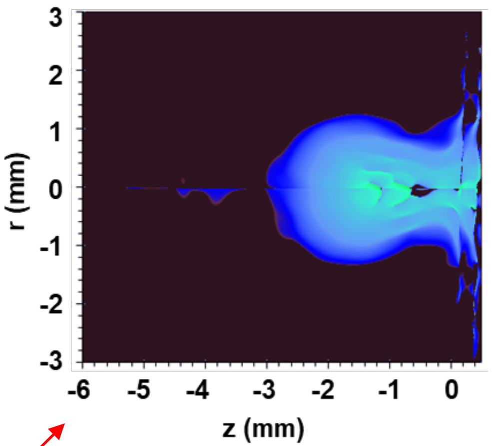

$$n(r) = \frac{-2n_c}{\pi\omega}\int_r^a \frac{d\Delta\phi}{dh}\frac{dh}{\sqrt{h^2-r^2}}$$

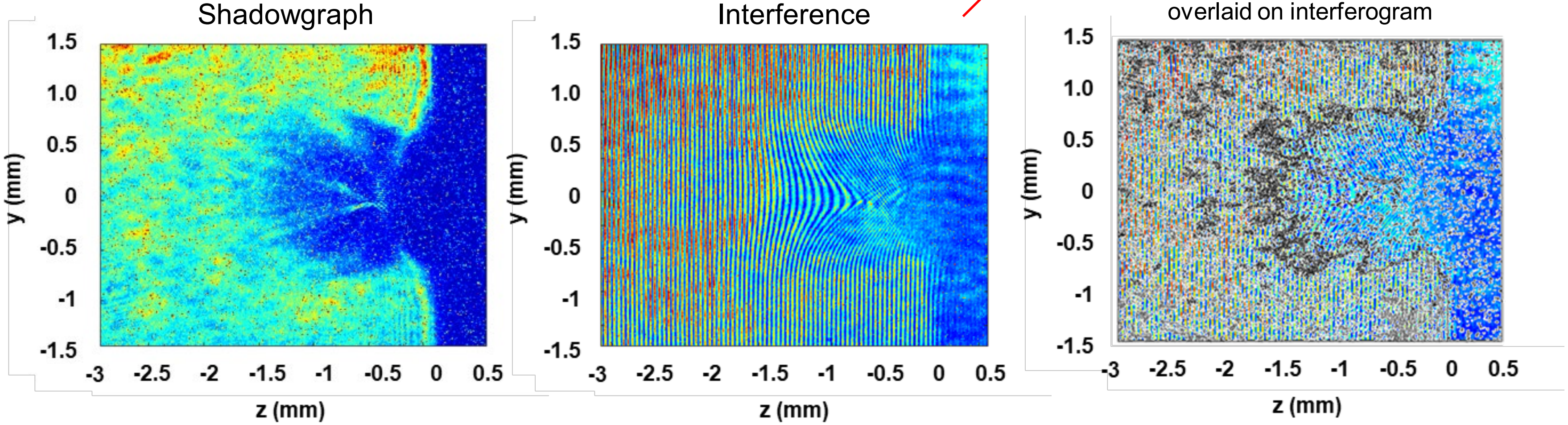

J.E. Coleman et al., J. Appl. Phys. **131**, 215901 (2022).

First spatiotemporal resolved electron density measurement with intense electrons

Biermann-battery may be "pinching" the plume near the foil surface and generating ejecta.

Spontaneous (thermal) B-fields were first observed in laser-produced plasmas by Stamper [1] and Colombant [2].

[2,3] $$\frac{\partial \vec{B}}{\partial t} = \nabla \times (\vec{v} \times \vec{B}) - \frac{1}{en_e} \nabla n_e \times \nabla T_e$$

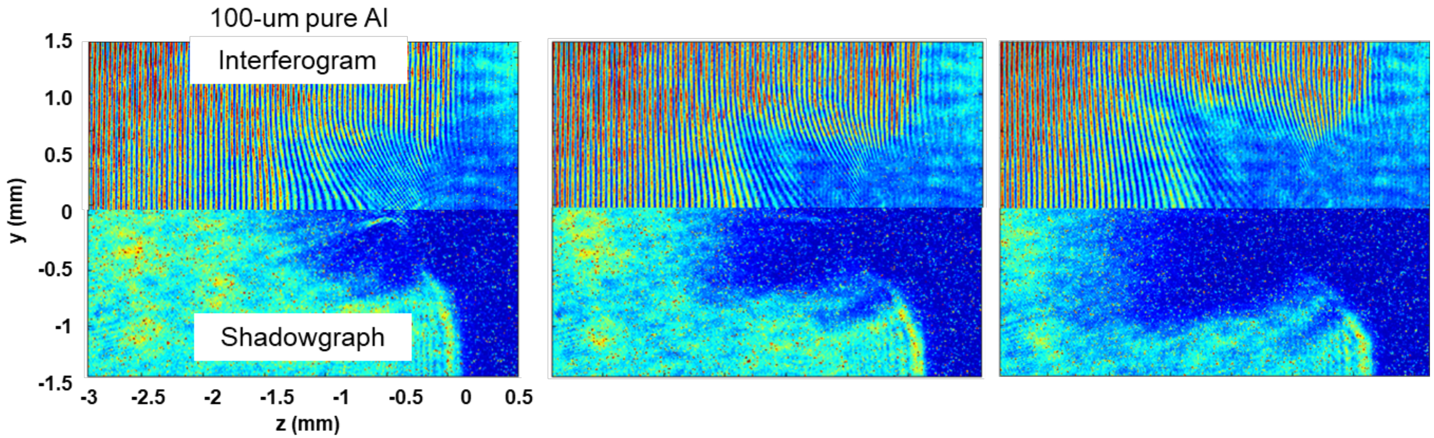

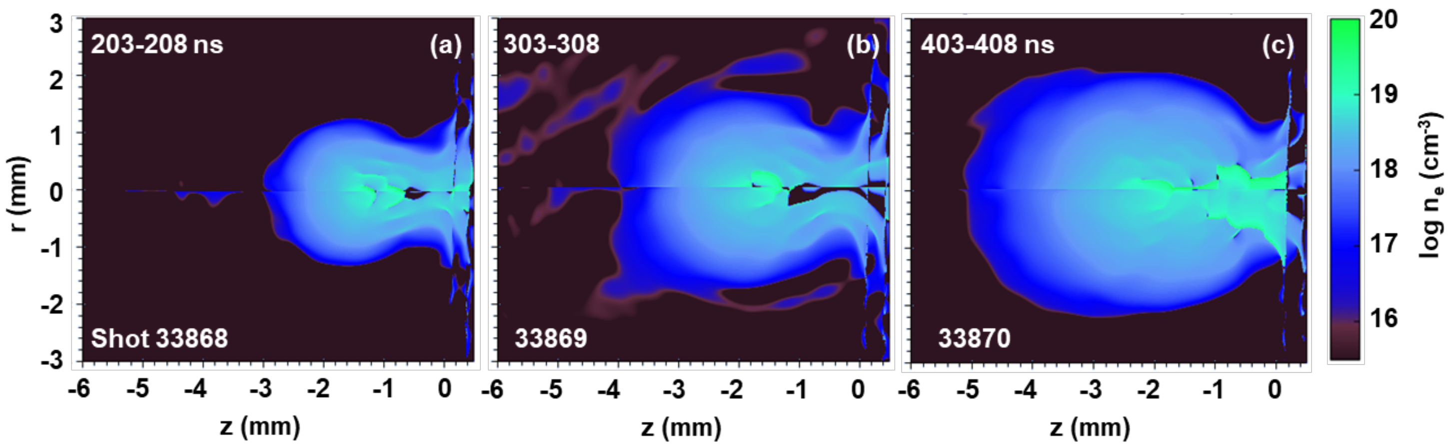

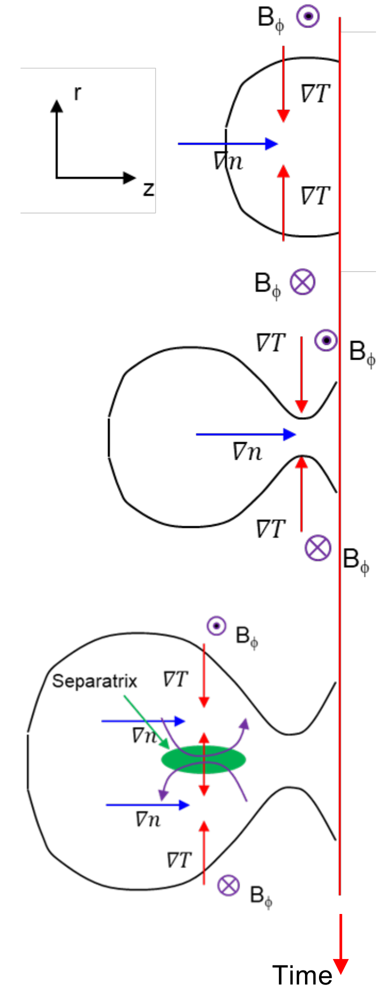

[1] J.A. Stamper et al., Phys. Rev. Lett **26,** 1012 (1971).
[2] D.G. Colombant et al., Phys. Rev. Lett **38,** 697 (1977).
[3] C.K. Li et al., Phys. Rev. Lett **97,** 135003 (2006).
[4] J.E. Coleman et al., J. Appl. Phys. **131**, 215901 (2022).

We are developing diagnostics to properly interpret the complex physics phenomena we observe.

Shot 33944, 300 ns, 100 um Sn

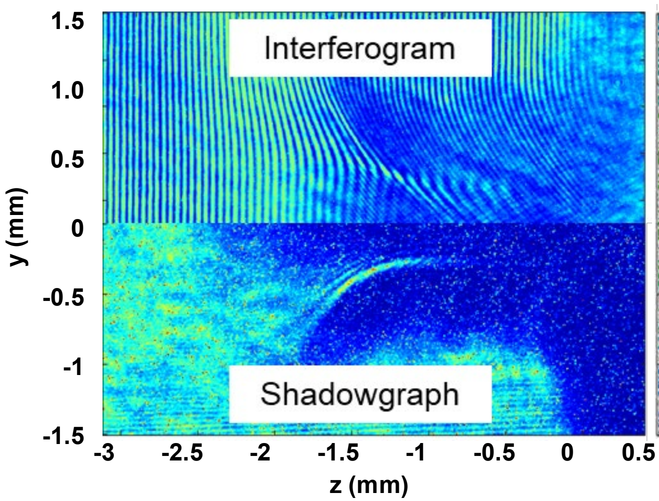

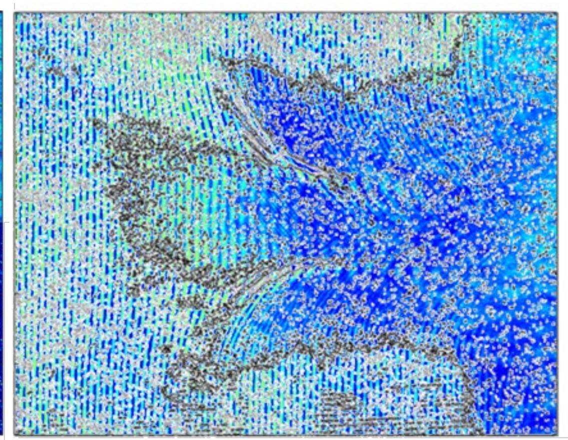

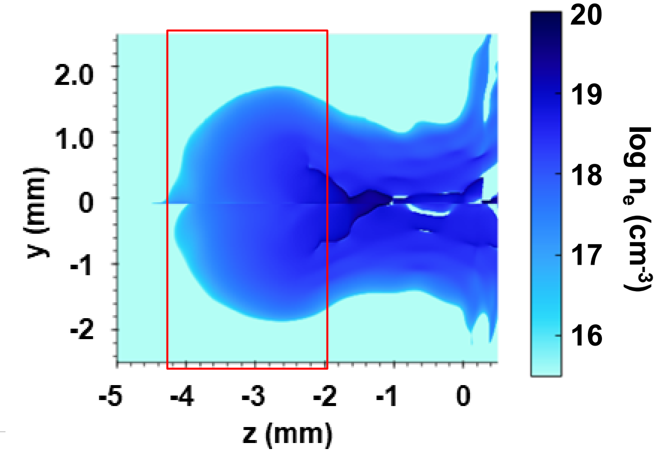

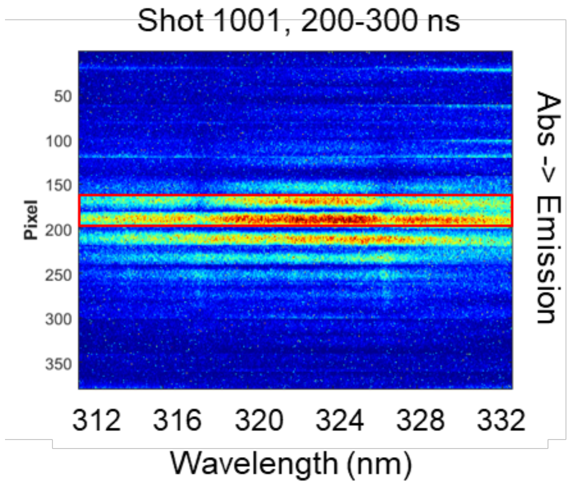

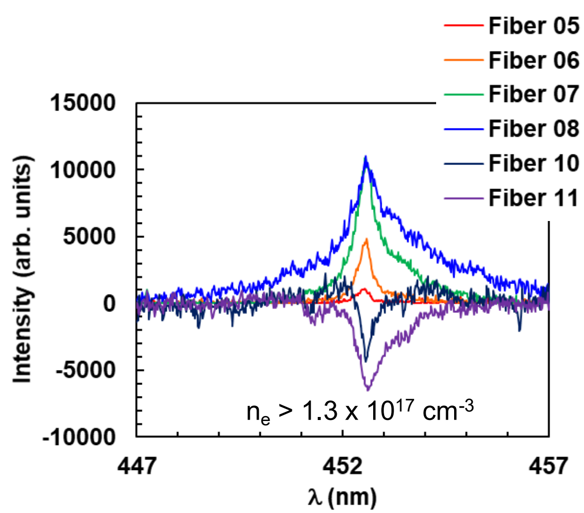

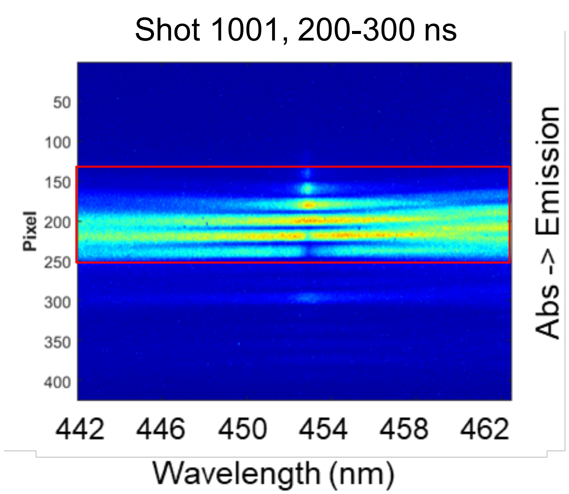

J.E. Coleman, et al. Phys. Plasmas **24**, 083302 (2017).
N.B. Ramey, et al., Phys. Plasmas **28**, 033301 (2021).

Radiation transport models must be used to interpret the spectroscopy results

LANL should have an electron beam facility dedicated to beam dynamics & target studies => laboratory astrophysics and WDM.

We have an 3.5 MV Blumlein injector

4 solenoids for transport and final focus

Beam parameters: 3-3.5 MeV, 1.0-1.4 kA

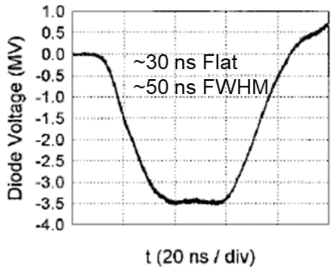

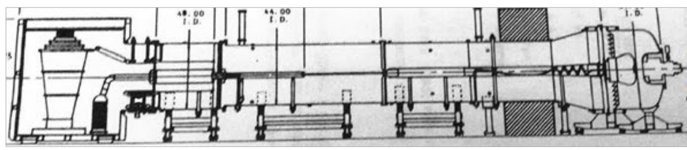

SLIA 3 MV, ~30 ns transmission line injector [1]

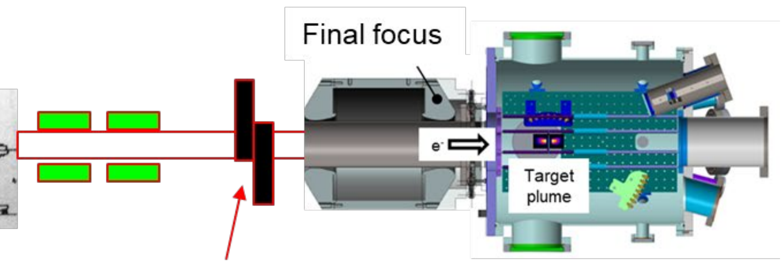

Energy (MeV)	Current (kA)	J (A/cm2)	γ	β	K
3	2.05	104.41	6.871	0.9894	7.66E-04
2	1.2	61.12	4.914	0.9791	1.27E-03
1	0.45	22.92	2.957	0.9411	2.45E-03

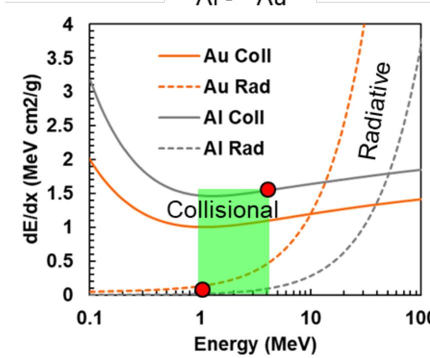

5 cm cathode, ~13 cm AK gap

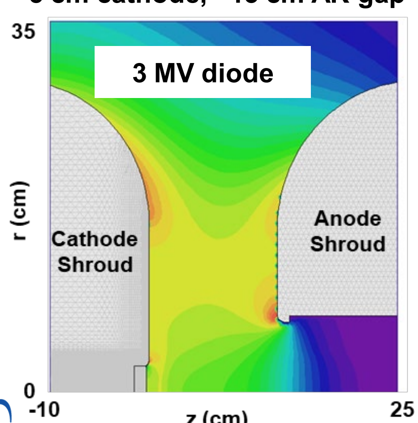

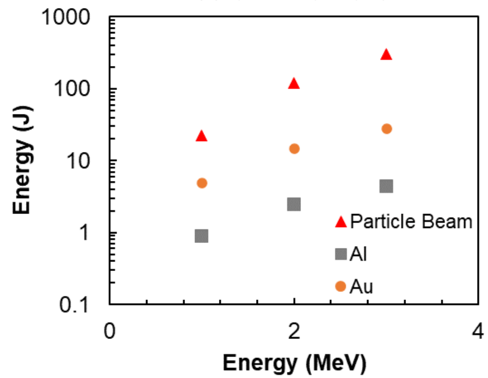

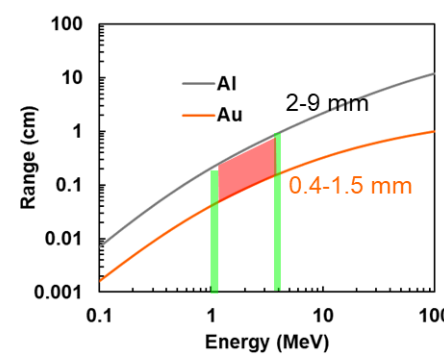

Los Alamos NATIONAL LABORATORY EST.1943

[1] J.R. Smith et al., In Proceedings of the Particle Accelerator Conference, 1997 p. 1251.

Conclusions

- **Intense electron beams are not difficult to produce**
  - Field emission (poor ε) and thermionic cathodes (poor J) do the job today
  - Higher brightness cathode technologies are under development
- **Small hollow cathodes exhibit potential diocotron unstable distributions.**
- **Non-linear transport effects likely degrade our beam quality and increase emittance.**
- **e- provide an advantageous heating (energy deposition) technique which can be utilized for a wide range of material studies**
  - X-ray production, η(material, Δz)
  - Neutron production, η(material, photofission σ, Δz)
  - electrical and thermal conductivity - WDM
  - Vapor dome equation-of-state, WDM

Physics challenges for advanced radiography

END

As the target begins to hydrodynamically disassemble it transitions through the warm dense matter regime.

WDM is a **low-temperature plasma** at nearly **solid density** covering the parameter space of $0.1 < T_e$ (eV) < 10 and $10^{22} < n_e$ (cm−3) $< 10^{24}$ for most metals. WDM is typically strongly coupled ($\Gamma \sim 1$) and degenerate due to the Fermi energy >1 eV compared to lower-density classical plasmas [1–3].

Phase diagram

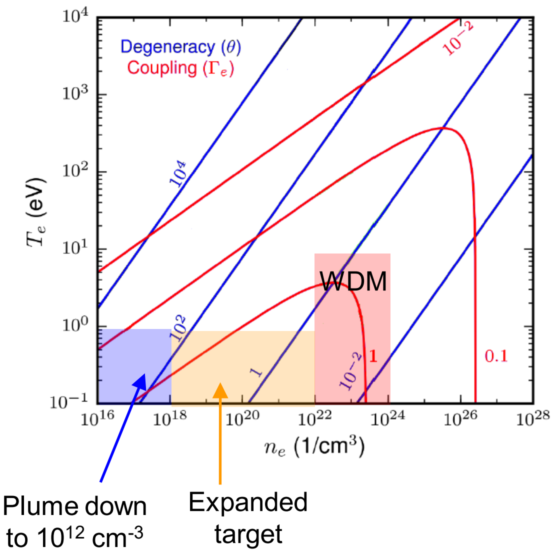

Coupling $$\Gamma = \frac{q^2\left(\frac{4\pi n_e}{3}\right)^{1/3}}{4\pi\varepsilon_o(T_e + E_F)}$$

Degeneracy $$\theta = \frac{T_e}{E_F}$$

Coupling – ratio of interaction energy between the particles : combine kinetic and quantum energy.

Degeneracy – quantifies ionization vs. quantum excitation.

Fermi Energy $$E_F = \frac{\hbar^2}{2m_e}(3\pi^2 n_e)^{2/3}$$

Atomic density

$$n_o = \frac{\rho N_A}{M}$$

[3] A.B. Zylstra et al., PRL **114**, 215002 (2015)

Fermi energy: ΔE between the highest and lowest occupied quantized states.

WDM is spatially localized and finite in time. The lifetime can be estimated by hydro simulations, but needs to be confirmed by measurements.

[1] *Committee on High Energy Density Plasma Physics, National Research Council, Frontiers in High Energy Density Physics: The X-Games of Contemporary Science* (The National Academies Press, Washington, DC, 2003).
[2] R.W. Lee, et al., J. Opt. Soc. Am. B **20**, 770 (2003).

We are continuing to advance our radiation transport models in order to better interpret our spectroscopy measurements.

Incoming beam parameters: 19.8 MeV, 1.45 kA, FWHM = 0.62 mm

Radiation transport process

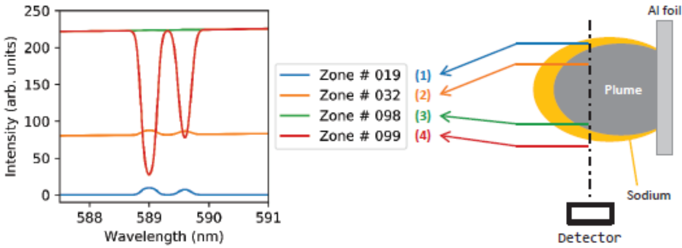

100-um Al1100, Shot 28890, 200-300 ns

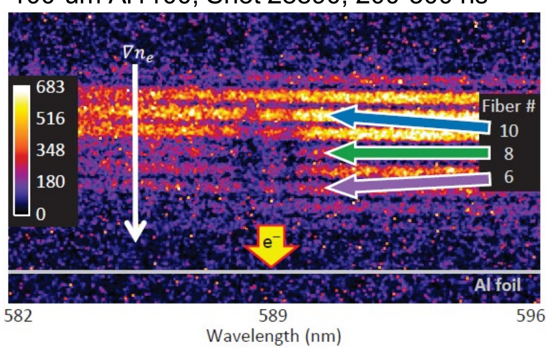

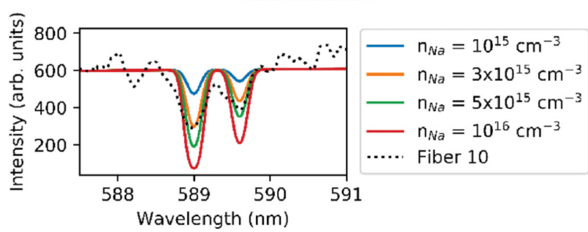

Absorbed Na lines on a dense Al continuum

n_{Al} = 1.1 x 10^{21} cm^{-3}, Z = 0.48

N.B. Ramey, J.E. Coleman, et al., Phys. Plasmas **28**, 033301 (2021).

100-um Anodized Al, Shot 32044, 100-300 ns

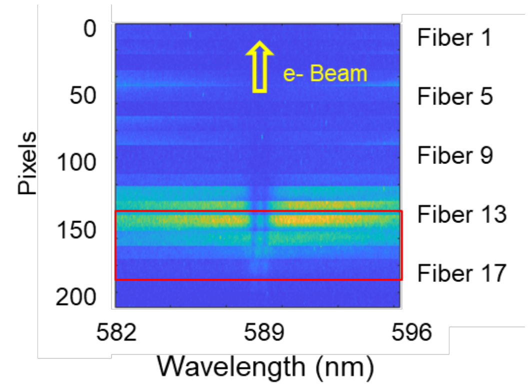

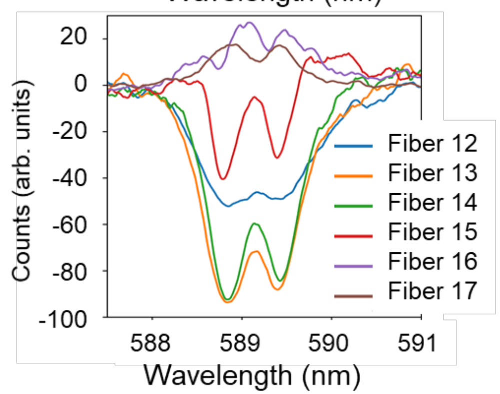

100-um Sn, Shot 1001, 200-300 ns

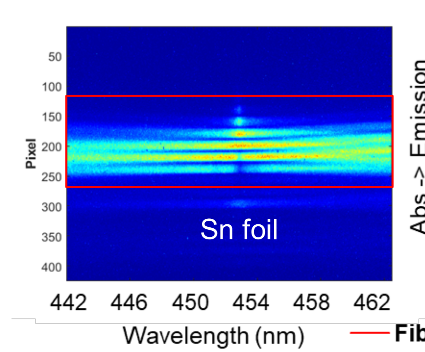

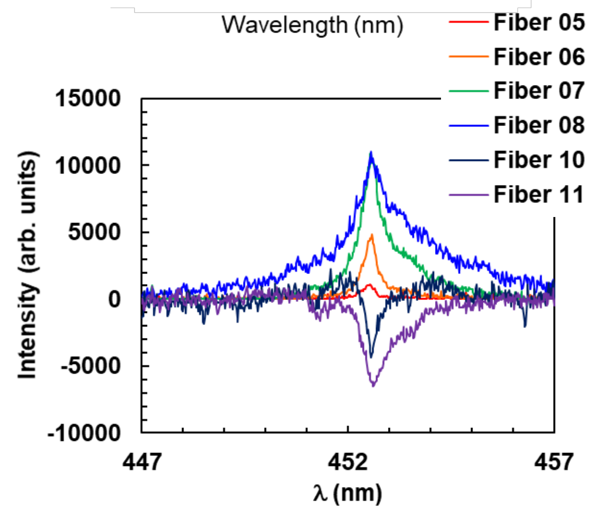

Stark widths indicate

n_e > 1.3 x 10^{17} cm^{-3}

~3.5 mm upstream

As we increase in Z the energy levels increasing the complexity.